Structure and magnetic properties of RCu$_4$Mn (R=La–Gd)

S. K. Dhar,[1] R. Kulkarni,[1] P. Manfrinetti,[1,2] M. L. Fornasini,[2] and C. Bernini[3]
[1]*CMP&MS Group, TIFR, Homi Bhabha Road, Mumbai 400 005, India*
[2]*Dipartimento di Chimica e Chimica Industriale, Università di Genova, Via Deodecaneso 31, 16146 Genova, Italy*
[3]*CNR-INFM-LAMIA Laboratory, Corso Perrone 24, 16152 Genova, Italy*
(Received 24 November 2007; published 20 February 2008)

We report the synthesis of new alloys of composition RCu$_4$Mn for R=La, Ce, Pr, Nd, Sm, and Gd. The ternary compounds are found to crystallize in the hexagonal CaCu$_5$-type structure of the RCu$_5$ parent compounds, but for the Gd compound, this proved to be the high-temperature form. X-ray diffraction on a single crystal of GdCu$_4$Mn was used to determine the site occupancies. The Mn ions substitute randomly on the Cu sublattice. The magnetization, electrical resistivity, and the heat capacity data show the absence of long range magnetic order in all the alloys in marked contrast to the parent RCu$_5$ (R=Ce, Nd, Sm, and Gd) compounds which order magnetically. A complex, inhomogeneous magnetic state arising from the Cu-Mn disorder and 3d-3d and 3d-4f interactions is proposed.

DOI: 10.1103/PhysRevB.77.054424 PACS number(s): 75.50.Lk, 75.20.En, 75.40.Cx

I. INTRODUCTION

The rare earths (R) form a number of compounds at the stoichiometry RT_5 with the hexagonal CaCu$_5$-type structure, where T is a transition element, such as Co, Ni, Cu, and Pt. In normal conditions, the hexagonal RCu$_5$ phase forms only for R=La-Eu and Y, while for R=Dy-Tm and Lu, the cubic AuBe$_5$ structure is adopted.[1] For R=Gd and Tb, both structures are found, the hexagonal GdCu$_5$ being a high-temperature phase. The substitution of some other elements for copper leads in some cases to compounds crystallizing in the MgCu$_4$Sn prototype (a ternary variant of AuBe$_5$), for instance, YbCu$_4M$ (M=In, Ni, Pd, Zn, Cd, Mg, Tl, Au, and Ag),[2–4] although YbCu$_5$ does not form under normal conditions. Some of these Yb compounds show strongly correlated electron behavior arising from the hybridization between the Yb 4f and the conduction band electron states.[2–6] RCu$_4$In compounds (R=Nd, Sm, Gd-Lu, Y) (Ref. 7) also adopt the cubic MgCu$_4$Sn-type structure and show interesting magnetic and transport properties, such as semi-metallic-like behavior in Y and Gd analogs and exchange frustrated antiferromagnetism in GdCu$_4$In.[8,9] While isostructural PrNi$_5$ and PrCu$_5$ are Van Vleck paramagnets, it has been reported that their solid solutions PrNi$_{5-x}$Cu$_x$ are ferromagnets for intermediate copper concentration, tentatively attributed to an enhanced f-f exchange interaction induced by an enhancement of 3d band susceptibility.[10] The cubic CeNi$_4$Mn, derived from hexagonal CeNi$_5$ by partially substituting Mn for Ni, has recently been identified as a soft ferromagnet (T_c ~150 K) with a high degree of transport spin polarization (~66%), the latter being a key desired property of spintronics materials.[11] Antiferromagnetic ordering has recently been reported in GdCu$_4$Al and GdCu$_4$Ga, crystallizing in the CaCu$_5$ type, with substitution of Cu by Al or Ga preferentially on the 3g site.[12]

Keeping in mind the above observations which point out the tendency of RT_5 compounds toward a structural transformation on partial substitution of T atom and the interesting magnetic and strongly electron correlated properties of the derivative ternary compounds, we have studied in this work the RCu$_4$Mn compounds with R=La, Ce, Pr, Nd, Sm, and Gd.

II. EXPERIMENTAL

The metals used were commercial products with high purity (99.9 wt. % for the rare earths, R; 99.999 and 99.99 wt. % for Cu and Mn, respectively). To avoid any weight losses due to possible volatilization of manganese during reaction and melting because of the high vapor pressure of this metal, the alloys were prepared in sealed crucibles. The weighed amounts of the metals (in the form of freshly prepared turnings for R and Cu and of very small grains for Mn; total mass of about 5 g) were pressed together directly into outgassed tantalum crucibles which were sealed by arc welding under a pure Ar flow. Samples were then melted by heating the crucibles in a high-frequency induction furnace up to 1150–1200 °C, shaken to ensure homogenization and remelted twice. The highest temperature of 1200 °C in the synthesis of these compounds was adopted after reactivity toward the container metal was noticed when the liquid alloys were brought to temperatures higher than 1250 °C.

The crucibles were then sealed under vacuum in quartz tubes and the samples annealed in resistance furnaces at 800 °C (details of the thermal treatments are given in Table I). Quenching, when adopted, was performed by suddenly breaking the ampoule in an ice-water bath. Differential thermal analysis (DTA) was done on La, Sm, and Gd analogs to determine the liquidus, the type, and the formation temperature of the phase RCu$_4$Mn and to check for a possible structural transformation. Specimens of the alloys prepared as above (about 0.8 g) and closed by arc welding into Mo crucibles were transferred to the DTA equipment and subjected to heating and cooling cycles at the rates of 5 or 10 deg/min, the temperature measurements being accurate to within ±5 °C.

Metallographic examination was performed by both optical and electron microscopies and the semiquantitative analysis of the phases was performed by microprobe. X-ray

TABLE I. Thermal treatment, lattice parameters (from the Guinier powder pattern), unit cell volume (V_u), and mean atomic volume ($V_{at.}$) for the $CaCu_5$-type RCu_4Mn compounds (R=La-Nd,Sm,Gd)..

Compound	Thermal treatment	Lattice constants (Å)				
		a	c	c/a	V_u (Å^3)	$V_{at.}$ (Å^3)
$LaCu_4Mn$	800 °C-13 days, air cooled	5.255(1)	4.180(1)	0.795	99.96	16.66
$CeCu_4Mn$	800 °C-9 days, air cooled	5.172(1)	4.119(1)	0.796	95.42	15.90
$PrCu_4Mn$	800 °C-12 days, air cooled	5.196(1)	4.168(1)	0.802	97.45	16.24
$NdCu_4Mn$	800 °C-9 days, air cooled	5.176(1)	4.171(1)	0.806	96.77	16.13
$SmCu_4Mn$	800 °C-7 days, water quenched	5.144(1)	4.161(1)	0.809	95.35	15.89
$GdCu_4Mn$	800 °C-13 days, water quenched	5.112(1)	4.160(1)	0.813	94.37	15.73

analysis was carried out on powders and a single crystal. Powder patterns were obtained by a Guinier-Stoe camera or a Bragg-Brentano diffractometer, using the Cu $K\alpha$ radiation and pure Si as an internal standard (a=5.4308 Å); the Guinier patterns were easily indexed according to the hexagonal $CaCu_5$-type cell and the lattice parameters determined by the least squares methods. Reflection intensities obtained on a tiny $GdCu_4Mn$ single crystal, isolated from the alloy annealed at 800 °C and quenched, were collected at 293 K on a Bruker-Nonius MACH3 diffractometer with graphite-monochromated Mo $K\alpha$ (λ=0.7107 Å) and its lattice parameters obtained from 25 diffractometer-measured reflections at θ=32°–34°. Absorption effects were corrected by ψ-scan data of the three top reflections and the structure was refined using F_0^2 with SHELXL-97.[13]

Magnetization was measured in a superconducting quantum interference device (Quantum Design) magnetometer. Heat capacity data were collected using the semiadiabatic, heat pulse method; a Lake Shore germanium resistance thermometer was used as the temperature sensor and a strain gauge as the heating element, both glued with GE varnish to a thin copper disk which also accommodates the sample coated with a thin layer of Apiezon grease. Resistivity measurements were carried out by the four-probe dc method using typically a current of 50 mA; a Lake Shore silicon diode was used to measure the temperature.

III. RESULTS

A. Phase stability and crystal structure

DTA results on $LaCu_4Mn$, $SmCu_4Mn$, and $GdCu_4Mn$ show that the compounds form congruently from the liquid; very likely, the other three compounds with R=Ce, Pr, and Nd also melt congruently. Figure 1 shows a typical cooling DTA run (10 °C/min) for $LaCu_4Mn$. The strong peak at higher temperature (arising due to the melting transition) is followed by a second, relatively weak, thermal effect at about 735, 810, and 800 °C, for La, Sm, and Gd specimens, respectively. To verify whether the weak thermal effect in these alloys was associated with any structural transformation, a series of annealing treatments at different temperatures was tried, i.e., 770 °C-14 days+quenching, 700 °C-5 days+quenching, 600 °C-7 days+air cooling, 500 °C-14 days+quenching, and 500 °C-8 days+air cooling (the latter two only for the Gd compound). From an examination of powder patterns, it is found that $LaCu_4Mn$ and $SmCu_4Mn$ retain their hexagonal $CaCu_5$-type structure down to room temperature. $GdCu_4Mn$, however, is no longer stable below 700 °C and converts into a phase which maintains the $CaCu_5$-type structure but with a lowering of both lattice parameters, accompanied with a small amount of a new compound with composition close to $RCu_{4.7}Mn_{1.3}$ (Ref. 14) and a structure related to the $YbMo_2Al_4$ type. The weak thermal effect in the DTA of $GdCu_4Mn$ is most likely associated with the formation of the latter minor phase.

Based on the powder patterns obtained on test charges with different heat treatments, an annealing temperature of 800 °C was chosen and the resulting single or nearly single phase samples were used for the investigation of their magnetic properties. The thermal treatment and the lattice parameters of the six RCu_4Mn compounds crystallizing in the $CaCu_5$-type structure are listed in Table I. The powder diffraction pattern of $SmCu_4Mn$ is shown in Fig. 2. Similar patterns were obtained for the other compounds.

Single crystal data of $GdCu_4Mn$ were used to refine the Cu/Mn occupancies, obtaining the same random distribution on both non-rare-earth sites with a ratio Cu/Mn=4 within

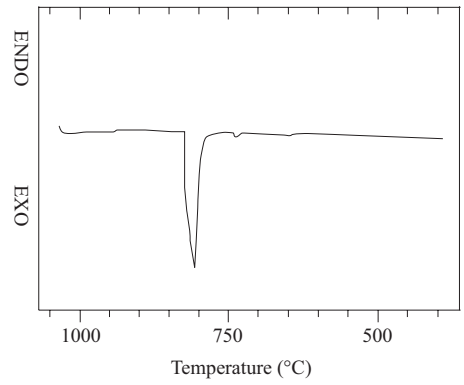

FIG. 1. The DTA curve of $LaCu_4Mn$ recorded on cooling at 10 °C/min. The pronounced peak at 825 °C is due to the congruent solidification of $LaCu_4Mn$. The small peak at 735 °C can be ascribed to the formation of a phase with approximate composition $LaCu_{4.7}Mn_{1.3}$.

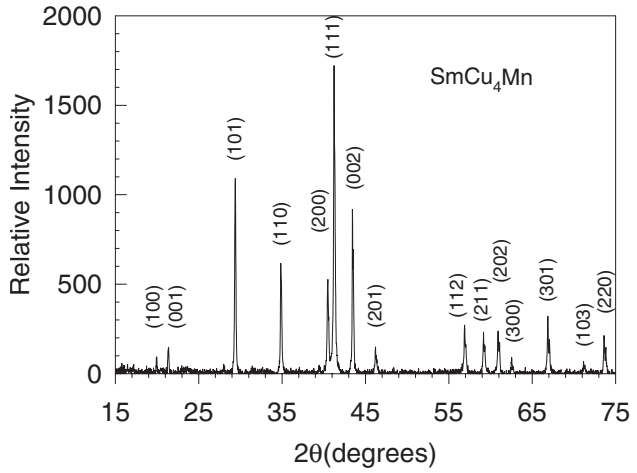

FIG. 2. Powder diffraction pattern of $SmCu_4Mn$.

two standard uncertainties. Therefore, in the last refinement cycles, the occupancies were fixed to 80% Cu+20% Mn for both sites. Although the atomic numbers of Mn and Cu differ only by four units, we have shown earlier in the crystal structure refinement by the x-ray data of some Ce-Cu-Mn compounds that it is possible to distinguish between sites occupied only by copper or manganese and sites with mixed Cu/Mn occupancy.[14] Following the results recently reported for $GdCu_4Al$,[12] a trial run was carried out by filling the $2c$ sites with Cu and the $3d$ sites with a Cu/Mn mixture. However, agreement factors and standard uncertainties worsened significantly. Details on the data collection and refinement of $GdCu_4Mn$ can be obtained from the authors on request. The atomic coordinates and equivalent isotropic displacement parameters are shown in Table II. In the $GdCu_4Mn$ structure, the Cu/Mn atoms form regular trigonal bipyramids joined through their vertices, with practically the same Cu/Mn-Cu/Mn distances. [2.550(1)–2.553(1) Å]. The Gd atoms fill the voids within the three-dimensional Cu/Mn framework.

B. Magnetic properties

Figure 3 shows the thermal variation of the magnetization of $LaCu_4Mn$ measured in both the zero-field-cooled (ZFC) and field-cooled (FC) states in an applied field of 100 Oe. Since both La and Cu are nonmagnetic, the magnetic behavior of $LaCu_4Mn$ can be ascribed solely to the Mn ions. The magnetization shows a peak at 35–36 K with a magnitude of 0.05 emu/mol. There is a pronounced difference between the

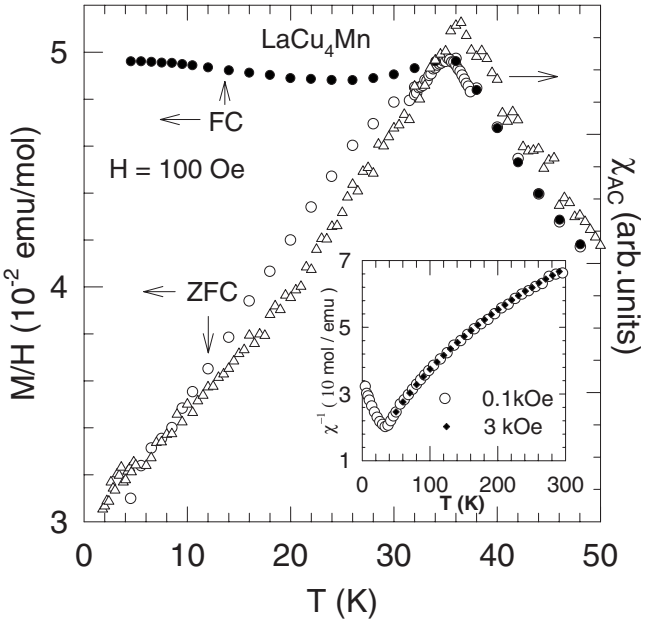

FIG. 3. The ZFC and FC magnetizations of $LaCu_4Mn$ in a field of 100 Oe. χ_{ac} is also plotted. The inset shows the χ^{-1} measured in applied fields of 0.1 and 3 kOe. The solid line is a fit to the data.

ZFC and FC data at temperatures below the peak. These features of the low-field magnetization are typical characteristics of a spin glass transition and suggest a random freezing of the Mn ions below the peak temperature. The absence of any anomaly in the heat capacity data (see below) further reinforces the conclusion derived from the magnetization data. The ac susceptibility χ_{ac} data taken at 31 Hz with $H_{ac} \sim 1$ Oe are also shown in the figure. The peak in the χ_{ac} is shifted up in temperature by nearly 1 K compared to the peak position in the dc magnetization measured in 100 Oe.

The inverse susceptibility χ^{-1} (measured in applied fields of 0.1 and 3 kOe) plotted in the inset of Fig. 3 does not show a linear variation with temperature in any extended range between the peak temperature and 300 K and thus shows a behavior similar to that reported earlier in spin glasses ThMnAl, YMnAl,[15] NdMnAl, and *R*MnIn and related compounds.[16,17] In ThMnAl, a modified Curie-Weiss expression $\chi = C_{CW}/(T-\theta_p)+\chi_0$, where χ_0 is temperature independent, was fitted to the data. Applying the same procedure here gives the following values for the paramagnetic effective moment μ_{eff} derived from C_{CW}, the paramagnetic Curie temperature θ_p, and χ_0: $\mu_{eff}=4.43$ and 4.36 μ_B, $\theta_p=-25.8$ and −22.5 K, and $\chi_0=7.24\times10^{-3}$ and 7.42×10^{-3} emu/mol

TABLE II. Atomic coordinates and equivalent isotropic displacement parameters for $GdCu_4Mn$.

Atom	Position	x	y	z	U_{eq} (Å^2)
Gd	$1a$	0	0	0	0.0114(3)
Cu1/Mn[a]	$3g$	1/2	0	1/2	0.0096(3)
Cu2/Mn[a]	$2c$	1/3	2/3	0	0.0102(3)

[a]Cu1/Mn, Cu2/Mn=0.8 Cu+0.2 Mn.

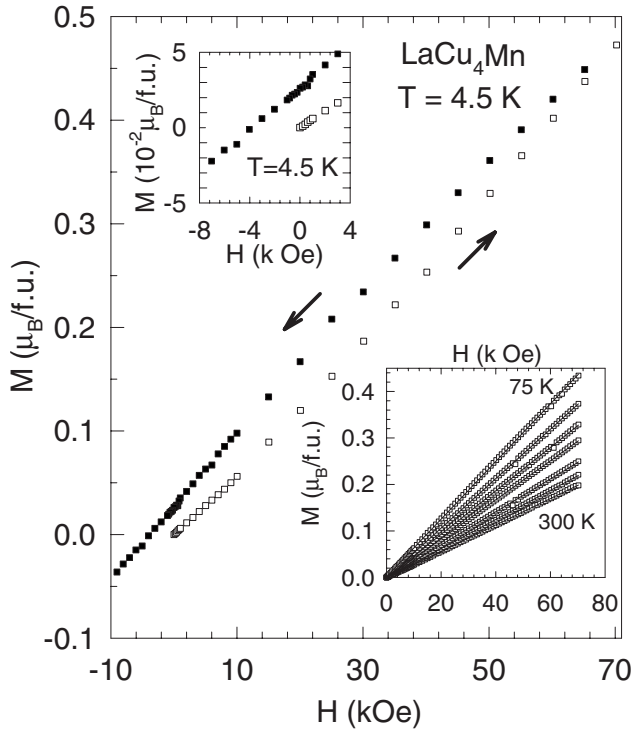

FIG. 4. The magnetization of $LaCu_4Mn$ at 4.5 K up to 70 kOe. The upper inset shows the low-field region on an expanded scale. The lower inset shows the isothermal magnetization at 75, 100, 125, 150, 200, 250, and 300 K.

in 100–300 and 50–300 K range, respectively. The fitted values of μ_{eff}, θ_p, and χ_0 are nearly independent of the temperature range of the fit. The value of μ_{eff} is less than 4.9(5.92) μ_B, the spin-only value for the Mn^{3+} $3d^4$ (Mn^{2+} $3d^5$) state, and can tentatively be explained by some degree of itinerancy of the Mn $3d$ state or incomplete quenching of the orbital angular momentum by the crystal electric fields. The paramagnetic Curie temperature θ_p is negative and on the same scale as the peak temperature of the magnetization. A negative θ_p indicates antiferromagnetic interactions between the Mn ions. However, the absence of a long range antiferromagnetic transition suggests a crossover from an antiferromagnetically correlated exchange at high temperatures to a frustrated one at low temperatures.

The isothermal magnetization of $LaCu_4Mn$ is shown in Fig. 4. At 4.5 K, the magnetization increases nearly linearly to a low value (relative to μ_{eff}) of about 0.5 μ_B/Mn ion at 70 kOe and shows hysteresis and a large coercive field of nearly 4 kOe, again reminiscent of the spin glass behavior. Above the peak temperature, the magnetization, measured at a few selected temperatures between 75 and 300 K, varies linearly with the applied field (lower inset, Fig. 4), as expected in the paramagnetic state.

Figures 5–11 show the temperature and field dependence of the magnetization in RCu_4Mn for R=Ce, Pr, Nd, Sm, and Gd, respectively. The ac susceptibility data ($H_{\text{ac}} \sim 1$ Oe) taken in nominal zero field for some compounds are also shown. In these compounds, the magnetic response arises from the magnetic moments associated with both the Mn

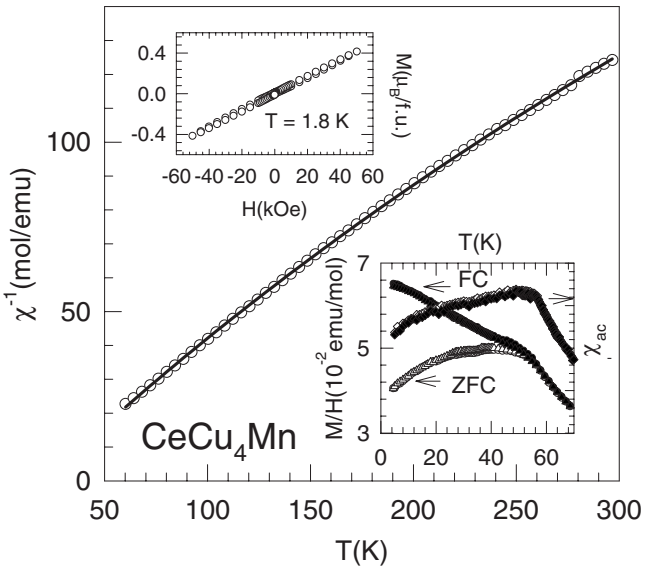

FIG. 5. The χ^{-1} of $CeCu_4Mn$ between 50 and 300 K in 1 kOe. The upper inset shows in-field magnetization at 1.8 K. The lower inset shows ZFC and FC dc magnetizations in 50 and 500 Oe and χ_{ac}.

ions (as for $LaCu_4Mn$ above) and the partially filled $4f$ shell of the R ions. The low-field, ZFC-dc magnetization in Ce, Pr, Nd, and Gd compounds shows a relatively broader peak, compared to $LaCu_4Mn$, while the corresponding FC magnetization below the peak temperature, unlike its behavior in $LaCu_4Mn$, keeps on increasing monotonically with decreasing temperature. The onset of the thermodynamic irreversibility in the magnetization sets in at temperatures higher than the peak temperature particularly in Ce, Pr, and Nd

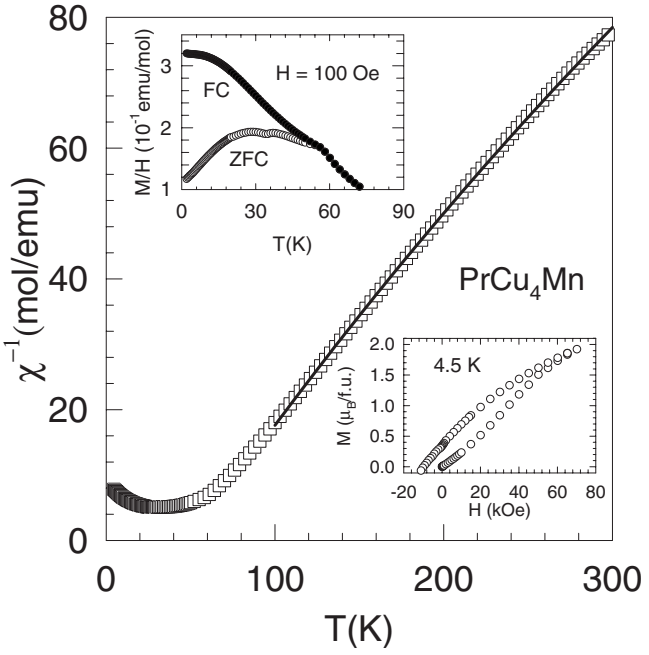

FIG. 6. The χ^{-1} of $PrCu_4Mn$ in 3 kOe. The ZFC and FC dc magnetizations in 100 Oe are shown in the upper inset. The lower inset shows a portion of the hysteresis curve at 4.5 K.

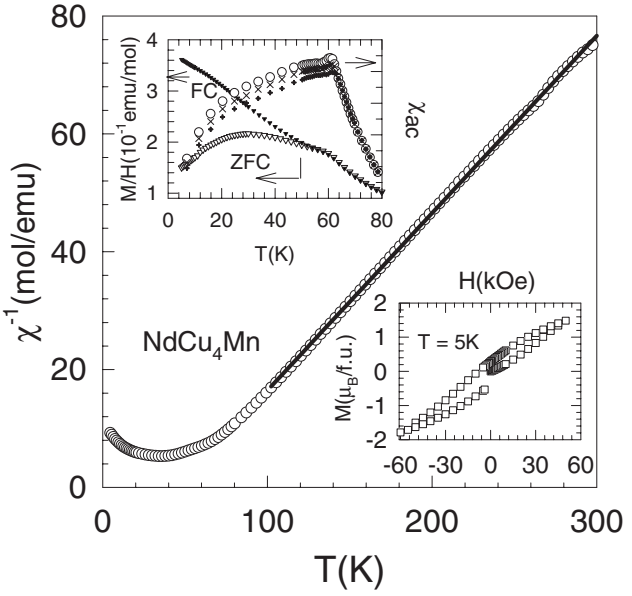

FIG. 7. The χ^{-1} of $NdCu_4Mn$ in 3 kOe. The ZFC and FC dc magnetizations in 100 Oe and χ_{ac} are plotted in the upper inset. The lower inset shows the hysteresis curve at 5 K.

analogs. The ac susceptibility χ_{ac} of $CeCu_4Mn$ shows a knee-like feature around the temperature where the irreversibility in the dc magnetization sets in and it does not exhibit any broad peak at lower temperatures. Similarly, a shallow peak in the χ_{ac} of $NdCu_4Mn$ occurs close to the temperature where a kink is seen in the low-field dc magnetization, the peak position shifting to higher temperatures as the frequency is increased. The dc magnetizations measured in 50 and 500 Oe in $CeCu_4Mn$ are nearly identical for ZFC and FC modes, respectively. On the other hand, in $GdCu_4Mn$ (Fig. 8), the

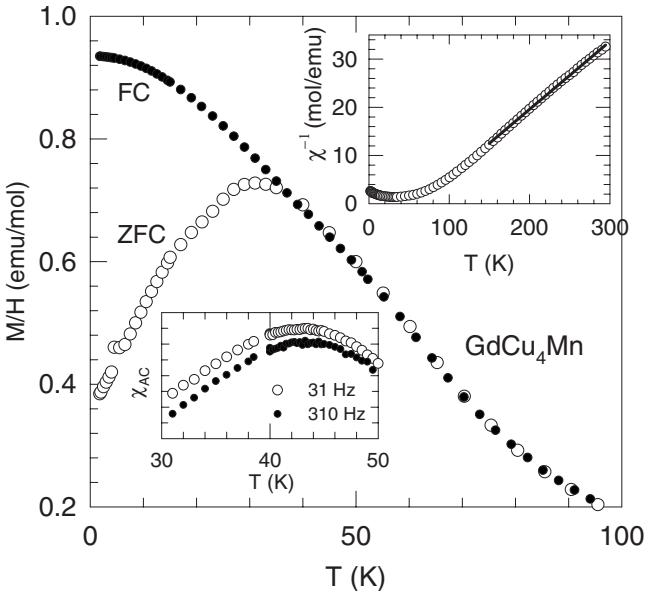

FIG. 8. The ZFC and FC magnetizations of $GdCu_4Mn$ in a field of 1 kOe. The lower inset shows the ac susceptibility at 31 and 310 Hz. The χ^{-1} up to 300 K is shown in the upper inset.

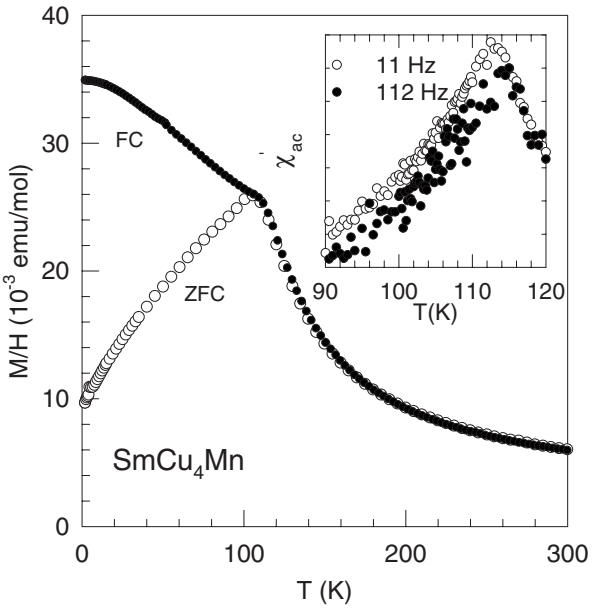

FIG. 9. The ZFC and FC magnetizations of $SmCu_4Mn$ in a field of 1 kOe. The inset shows the ac susceptibility at 11 and 112 Hz.

peak shifts appreciably to lower temperatures with increasing applied fields: from 43 K as measured in the χ_{ac} data to 31 K in the dc magnetization measured in an applied field of 1 kOe. Even a nominal dc field of 20 Oe (data not shown) shifts the peak down to 41 K. Similarly, the peak in the dc magnetization of $SmCu_4Mn$ occurs at 106 K in 1 kOe applied field, while the peak in χ_{ac} is seen near 113 K (inset of Fig. 9). The χ_{ac} data in $SmCu_4Mn$ were taken at 11 and 112 Hz. Like $NdCu_4Mn$, the χ_{ac} peak appears to be shifted upward in temperature at higher frequency which is a typical characteristic of the spin glass behavior. Due to the width of the transition as reflected in the χ_{ac} data of $GdCu_4Mn$, it is not possible to infer unambiguously whether there is any frequency dependent peak shift.

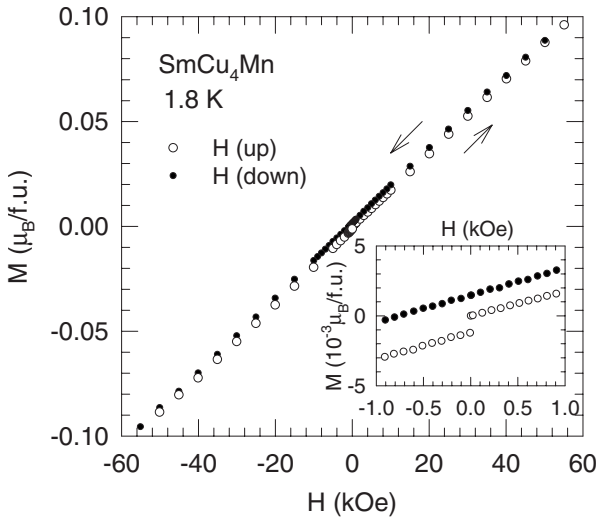

FIG. 10. The hysteresis loop of $SmCu_4Mn$ at 1.8 K. The inset shows the magnetization near the origin on an expanded scale.

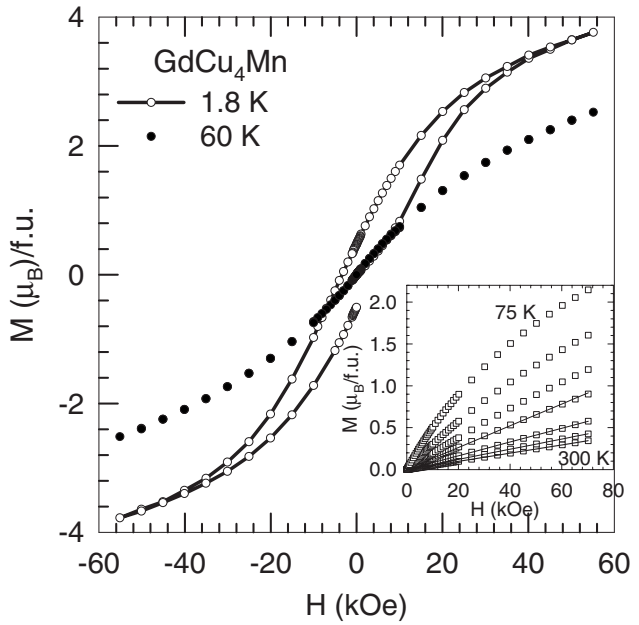

FIG. 11. The hysteresis loop of $GdCu_4Mn$ at 1.8 and 60 K. The inset shows the in-field magnetization at 75, 100, 125, 150, 200, 250, and 300 K.

The inverse susceptibility of RCu_4Mn (R=Pr, Nd, and Gd) shows a linear variation with the temperature in some range above 150 K depending on the rare-earth ion R. Accordingly, the Curie-Weiss expression $\chi=C_{CW}/(T-\theta_p)$ was fitted to the data, while an additional term χ_0 was added to the fitting expression for $CeCu_4Mn$. The fitted curve is drawn as a solid line through the data points (see figures). For $GdCu_4Mn$, the data in the temperature range of 250–350 K were used to derive the values for C_{CW} and θ_p from the fitting procedure. The values of μ_{eff}/f.u. (derived from the Curie constant C_{CW}) and θ_p are 3.75, 5.12, 5.15, and 8.1 μ_B and 20.4, 37.9, 45.3, and 30.1 K for Ce, Pr, Nd, and Gd analogs, respectively. For $GdCu_4Mn$, using the data in the range of 200–300 K results in a μ_{eff}/f.u. less than 7.94 μ_B, the paramagnetic moment of the free Gd^{3+} ion. Since μ_{eff}/f.u. in other RCu_4Mn compounds exceeds the corresponding value of the paramagnetic, free-ion moment, μ_R alone due to the contribution from the Mn ions, a similar situation is expected to hold in the Gd compound as well. An approximate value of μ_{Mn} in RCu_4Mn may be obtained by subtracting the contribution due to the free-trivalent rare-earth ion R. The values thus obtained are 2.8, 3.7, 3.7, and 1.9 μ_B per Mn ion in Ce, Pr, Nd, and Gd compounds, respectively. It is possible that μ_{Mn} in $CeCu_4Mn$ may be higher than 2.8 μ_B if the Ce ions in $CeCu_4Mn$ are in a valence fluctuating state such that their contribution to the magnetic susceptibility is diminished compared to that arising from the free-trivalent Ce ions assumed above. An indication of the anomalous valence state of the Ce ions is provided by the mean atomic volume V_u (see Table I) of $CeCu_4Mn$ which is less than that of $PrCu_4Mn$ and hence does not follow the normal lanthanide contraction behavior of the normal trivalent rare-earth ions. Unlike in $LaCu_4Mn$, θ_p is positive in these four compounds and indicates an overall ferromagnetic exchange interaction.

For the Sm compound, the inverse susceptibility (not plotted) shows a curvature at high temperatures like that in $LaCu_4Mn$ and $CeCu_4Mn$. The curvature may partly arise due to the same physical reasons as in the La and Ce compounds. However, in Sm^{3+} compounds, there is an appreciable nearly temperature independent Van Vleck contribution to the susceptibility arising from the excited levels of Hund's rule derived L-S multiplet structure due to a relatively small energy separation. Crystal fields can also admix the ground and the excited levels, thereby affecting the susceptibility. As a result, the susceptibility of Sm^{3+} compounds often does not show a Curie-Weiss behavior. In the parent $SmCu_5$, Svoboda *et al.* accounted for the deviation by invoking the crystal field mixing of $J=5/2$, $7/2$, and $9/2$ multiplet levels with an appropriate molecular field constant using a molecular field model.[18] An examination of the susceptibility data reported in the literature on the well known intermetallic compounds of Sm, including that of $SmCu_5$, shows that typically the value of susceptibility at 300 K (in the paramagnetic regime) is $\sim 1\times10^{-3}$ emu/mol. For $SmCu_4Mn$, $\chi(300\ K)=6\times10^{-3}$ emu/mol, indicating that the dominant contribution to the magnetization at 300 K is arising from the Mn ions ($\sim 5\times10^{-3}$ emu/mol). This is in conformity with the sizable μ_{eff} (Mn) found in $LaCu_4Mn$. Comparison with the susceptibility of $LaCu_4Mn$ at 300 K (nearly 15×10^{-3} emu/mol) suggests that the Mn magnetic moment decreases with the decrease in lattice volume, the latter arising due to the usual lanthanide contraction. This is in conformity with the lower values of μ_{eff} (Mn) obtained above in RCu_4Mn for R=Pr, Nd, and Gd compared to that in $LaCu_4Mn$. It has been observed previously that the lattice volume plays a role in determining the magnetic moment of Mn in RMn_2 compounds. The Mn magnetic moment decreases as the rare-earth atomic number increases from Pr to Dy and it is nearly equal to zero in Ho, Er, and Tm analogs of RMn_2 compounds.[19]

The low-temperature in-field magnetization of RCu_4Mn is characterized by a lack of saturation and hysteresis and is thus qualitatively similar to that of $LaCu_4Mn$. On reversal of the magnetic field, the magnetization of $CeCu_4Mn$, $PrCu_4Mn$, $NdCu_4Mn$, and $SmCu_4Mn$ changes sign at 1.5, 10, 8, and 0.7 kOe, respectively, which shows the existence of large coercive fields in these compounds. The in-field magnetization of $GdCu_4Mn$ measured at selected temperatures is shown in Fig. 11. Between 300 and 150 K, the plots are linear but below 150 K, they develop a mild curvature which increases with decreasing temperature. It may be noted that the nonlinearity in the isothermal magnetization sets in at temperatures much above the peak temperature. At 1.8 K, the magnetization at 55 kOe attains a value of nearly 4 μ_B/f.u. The magnetization exhibits a sizable hysteresis and the coercive field at 1.8 K is 3.5 kOe, which is similar in magnitude to that of $LaCu_4Mn$.

The heat capacity C data taken up to 50 K in $LaCu_4Mn$ and $GdCu_4Mn$ and up to 125 K in $SmCu_4Mn$ are partly shown in Fig. 12. The data do not exhibit any anomalies at temperatures corresponding to the peak in the magnetization data of La, Sm, and Gd compounds. For the sake of clarity, the C vs T data on $SmCu_4Mn$ are shown only between 100 and 125 K in the lower inset; at lower temperatures, they are comparable in magnitude to those of La and Gd analogs.

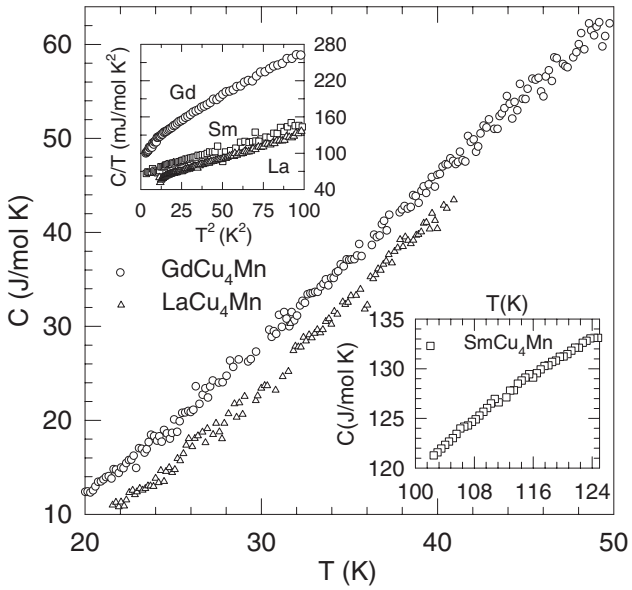

FIG. 12. The heat capacity C of $LaCu_4Mn$ and $GdCu_4Mn$ between 20 and 50 K. The lower inset shows the data for $SmCu_4Mn$ between 100 and 125 K; C/T vs T^2 up to 10 K on the three compounds is shown in the upper inset.

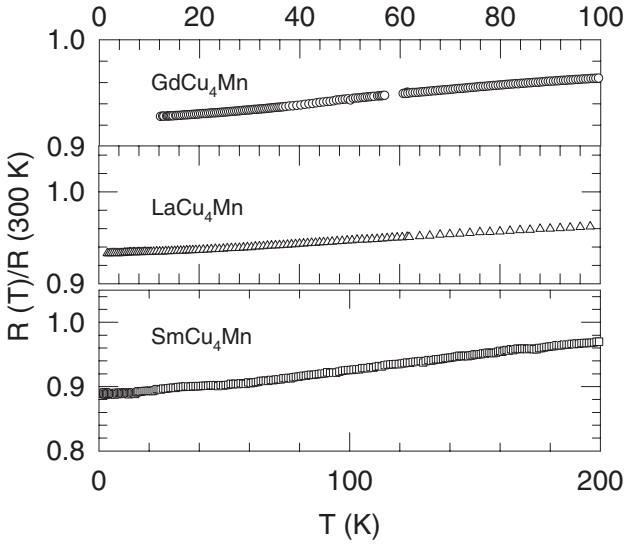

FIG. 13. The electrical resistivity of RCu$_4$Mn (R=La, Sm, and Gd).

Since the heat capacity shows a prominent peak at a long range magnetic transition, the data of Fig. 12 prove conclusively that the peaks in the magnetization in at least $LaCu_4Mn$, $SmCu_4Mn$, and $GdCu_4Mn$ are not associated with a long range magnetic order. We believe that a similar situation holds for Ce, Pr, and Nd analogs as well. The plots of C/T vs T^2 for $LaCu_4Mn$ and $SmCu_4Mn$ are practically linear below 10 K and give by extrapolation intercepts of 50 and 69 mJ/mol K^2 at 0 K, respectively. A similar procedure for the Gd compound in a restricted temperature range below 10 K gives an intercept of 113 mJ/mol K^2. These values are comparable to 65 and 50.2 mJ/mol K^2 obtained in ThMnAl and ThMnIn, respectively,[15] where the ground state shows inhomogeneous spin-glass-like properties. Since these values are obtained from extrapolating the data to $T=0$ K, they will include, besides the contribution due to the electronic density of states at the Fermi level, contributions arising from the magnetic degree of freedom associated with both the Mn and the rare-earth ions.

The thermal variation of the electrical resistivity for $T<200$ K, normalized to its value at 300 K for $LaCu_4Mn$ and $GdCu_4Mn$ and at 260 K for $SmCu_4Mn$, is shown in Fig. 13. The data for $SmCu_4Mn$ above 260 K have a large scatter. The residual resistivity in all the three compounds is large, between 150 and 200 $\mu\Omega$ cm, partly reflecting the Cu-Mn disorder. The resistivity shows a metallic behavior and varies smoothly, without any anomaly around the temperature where the peaks in the magnetization are found in the three compounds.

IV. DISCUSSION

The structural stability of binary AB_5 and ternary $A(B,B')_5$ intermetallic compounds (A=rare earth, alkaline earth, Zr, Hf, and Th; B=transition elements and/or p-block element such as Al, Ga, Sn, In, Si, and Ge) has recently been modeled in terms of three parameters: valence electron concentration (VEC), electronegativity difference, and the radius ratio R_A/R_B.[20] The RCu$_4$Mn have VEC=9 according to Ref. 20, where the values of full valences are used. While $LaCu_4Mn$ is inside the $CaCu_5$-type stability region of the plot, both $SmCu_4Mn$ and $GdCu_4Mn$ fall at the border between the $CaCu_5$ and $AuBe_5$ regions (Fig. 2 of Ref. 20), thus reflecting the same trend as found for the RCu$_5$ phases, where a coexistence of the two structural types starts just on gadolinium. In the $CaCu_5$ structure, the layers of Cu atoms at $3g$ sites are interspersed between the layers made up of Ca and Cu atoms at $1a$ and $2c$ sites, respectively. Single crystal data on $GdCu_4Mn$ presented above show that while the Gd, and most likely the other R atoms, form a regular periodic lattice in RCu$_4$Mn, the Mn ions are distributed randomly at the $2c$ and $3g$ sites.

With the exception of $LaCu_5$ which is a Pauli paramagnet, RCu$_5$ compounds for R=Ce,[21] Nd,[22] Sm,[18] and Gd (Ref. 23) exhibit a long range magnetic ordering at 3.8, 14.5, 9, and 25 K, respectively, the magnetic coupling between the R ions provided by the indirect Ruderman-Kittel-Kasuya-Yosida (RKKY) exchange interaction. While the magnetic ordering is antiferromagnetic in Ce, Sm, and Gd analogs, $NdCu_5$ orders ferromagnetically at 14.5 K and undergoes spin reorientation at a lower temperature. $PrCu_5$ is a Van Vleck paramagnet. A more recent work on $GdCu_5$ reports a T_N of 12.5 K.[24] In RCu$_4$Mn compounds, the presence of Mn ions will introduce additional $3d$-$3d$ and $3d$-$4f$ exchange interactions. Typically, the $3d$-$3d$ exchange interaction is much stronger than the $4f$-$4f$ interaction due to the direct $3d$-$3d$ overlap, though it may partly also be operating via the RKKY exchange. In $R\,3d$ compounds, it is not, therefore, unusual to find the $3d$ sublattice ordering magnetically at much higher temperature than the $4f$ sublattice. The peak in the magnetization of $LaCu_4Mn$ occurs at $\approx$36 K, higher than the Néel

temperature of $GdCu_5$. This indicates that the Mn-Mn exchange interactions are stronger than the *R*-*R* interactions in these alloys. Due to the random occupation of the Cu sites by the Mn ions, the exchange interactions between the Mn ions are frustrated. The nearest neighbor Mn-Mn distances in $GdCu_4Mn$, as inferred from the single crystal data, are 2.550 and 2.553 Å, respectively. It has been shown in α-Mn that the exchange interaction is antiferromagnetic for Mn-Mn distance less than 2.8 Å and ferromagnetic at longer distances.[25] Possibly, both the dominant antiferromagnetic and weaker ferromagnetic interactions between the Mn ions are operative in these alloys. The $4f$-$4f$ interaction, which leads to a long range magnetic order in the parent magnetic RCu_5, is apparently superseded in RCu_4Mn by the random exchange fields exerted by the Mn ions. The Mn ions at $2c$ and $3g$ sites are located at 2.948 and 3.294 Å, respectively, from the Gd ions, while the nearest Gd-Gd distance is 4.161 Å. Thus, the frustration and disorder on the Cu/Mn sublattice together with the relatively stronger $3d$-$4f$ (compared to $4f$-$4f$) interaction leads to an inhomogeneous magnetic state which partly shows a signature of spin-glass-like freezing of the magnetic ions, as evidenced by the pronounced difference in the ZFC and FC magnetizations below the peak temperature, low values of the low-temperature magnetization in fields as large as 70 kOe, hysteresis, and large coercive fields. The lack of an anomaly in the heat capacity data further corroborates the conclusion that an inhomogeneous magnetic state exists in these compounds.

The value of the paramagnetic moment μ_{eff}/f.u. in $GdCu_4Mn$ varies with the temperature range in which the Curie-Weiss expression is used to fit the data. It is even less than the free Gd-ion value of 7.94 μ_B when the data are fitted in the range of 200–300 K. One would expect a $\mu_{\text{eff}} > \mu_{\text{Gd}}$ due to the additional contribution from Mn ions. Qualitatively, one can explain such an observation by invoking the short range, nearest neighbor Gd-Mn antiferromagnetic coupling as the temperature is reduced below 300 K. However, μ_{eff}/f.u. $> \mu_R$ for other *R*. If the rare-earth spin *S* and the spin of the Mn ion couple antiferromagnetically for all *R*, then the Gd and Mn moments are coupled antiferromagnetically, while for the light rare earths, Ce to Sm, the moments are coupled ferromagnetically because the total angular momentum *J* for the light rare earths is given by $J=L-S$ with $L > S$ ($L=0$ for Gd and the crystal electric field effects are zero in the first approximation). The curved isotherms below 150 K in $GdCu_4Mn$, which can qualitatively be explained to arise due to the formation of superparamagnetic clusters, indicate a complex evolution of magnetic response with the decrease of temperature. A similar behavior has been seen earlier in the micromagnetic Cu-Mn alloys.[26] In quenched $Cu_{75}Mn_{25}$, the magnetization exhibits a peak at ~110 K due to the freezing of magnetic clusters. The isothermal magnetization plots above the peak temperature are curved up to about 190 K. A quantitative analysis of the temperature and field dependence of the magnetization of alloys with varying Cu/Mn ratio was explained by invoking the formation of superparamagnetic clusters. It may be noted that the peak temperature of the magnetization shifts considerably with the applied field particularly in $GdCu_4Mn$ and $SmCu_4Mn$. Such a shift in the peak of ZFC magnetization occurs in systems containing superparamagnetic clusters. Thus, the present data indicate a complex magnetic configuration in RCu_4Mn where we may have a short range *R*-Mn antiferromagnetic spin coupling at high temperatures, followed by the formation of superparamagnetic and spin-glass-like clusters with decreasing temperatures, depending on the near neighbor environment.

The FC magnetization in $LaCu_4Mn$ below the peak temperature is nearly pegged to its peak value, while for other *R* ions, it increases monotonically from its peak value down to the lowest temperature of 1.8 K. Thus, the presence of the magnetic rare-earth sublattice brings qualitative changes in the thermal variation of the FC magnetization. The freezing temperature in $SmCu_4Mn$, as deduced from the peak temperature of magnetization, is nearly three times larger compared to the corresponding value in $LaCu_4Mn$ and $GdCu_4Mn$. It is also much higher than the maxima seen in the χ_{ac} of $CeCu_4Mn$ and $NdCu_4Mn$ and the peak seen in the dc magnetization of $PrCu_4Mn$. The origin of this enhancement is not obvious. A study of $RCu_{5-x}Mn_x$ for various values of *x* may lead to a better understanding of the interplay between $3d$-$3d$ and $3d$-$4f$ interactions and the resultant variation in the magnetic behavior. It would be interesting to find how the long range magnetic order of the rare-earth sublattice is initially modified and then eventually broken up at higher *x*.

To conclude, we show in this paper that Cu can be replaced by Mn in RCu_5 compounds (*R*=La, Ce, Pr, Nd, Sm, and Gd) at least up to the composition RCu_4Mn, and the ternary alloys retain the $CaCu_5$-type hexagonal structure of the parent compounds. A single crystal study shows that the Mn atoms replace the Cu atoms at the two sites $3g$ and $2c$ of the RCu_5 unit cell randomly. The magnetization, heat capacity, and the resistivity data indicate an inhomogeneous magnetic ground state in all the three alloys, which arises due to the Cu-Mn disorder on the Cu sublattice and $3d$-$3d$ and $3d$-$4f$ interactions.

[1] P. Villars and L. D. Calvert, *Pearson's Handbook of Crystallographic Data for Intermetallic Phases*, 2nd ed. (ASM International, Materials Park, OH, 1991).

[2] C. Rossel, K. N. Yang, M. B. Maple, Z. Fisk, E. Zirngiebl, and J. D. Thompson, Phys. Rev. B **35**, 1914 (1987).

[3] K. Hiraoka, K. Kojima, T. Hihara, and T. Shinohara, J. Magn. Magn. Mater. **140-144**, 1243 (1995).

[4] J. L. Sarrao, C. D. Immer, Z. Fisk, C. H. Booth, E. Figueroa, J. M. Lawrence, R. Modler, A. L. Cornelius, M. F. Hundley, G. H. Kwei, J. D. Thompson, and F. Bridges, Phys. Rev. B **59**, 6855 (1999).

[5] J.-S. Kang, J. W. Allen, C. Rossel, C. L. Seaman, and M. B.

Maple, Phys. Rev. B **41**, 4078 (1990).
[6] J. L. Sarrao, Physica B **259-261**, 128 (1999).
[7] L. V. Sysa, V. I. Zaremba, Ya. M. Kalychak, and V. M. Baranyak, *Problems of Crystal Chemistry of Intermetallics Compounds and Chemical Analysis of Metals* (L'vov Vishcha Shkola, 1988), Vol. 29, p. 32–34.
[8] H. Nakamura, K. Ito, and M. Shiga, J. Phys.: Condens. Matter **6**, 9201 (1994).
[9] H. Nakamura, N. Kim, M. Shiga, R. Kmiec, K. Tomala, E. Ressouche, J. P. Sanchez, and B. Malman, J. Phys.: Condens. Matter **11**, 1095 (1999).
[10] A. G. Kuchin, A. S. Ermolenko, V. I. Khrabrov, G. M. Makarova, and E. V. Belozerov, J. Magn. Magn. Mater. **159**, L309 (1996).
[11] Surjeet Singh, G. Sheet, P. Raychaudhuri, and S. K. Dhar, Appl. Phys. Lett. **88**, 022506 (2006).
[12] S. Bobev, V. Fritsch, J. D. Thompson, and J. L. Sarrao, J. Solid State Chem. **179**, 1035 (2006).
[13] G. M. Sheldrick, SHELXL-97, program for refinement of crystal structures, University of Göttingen, Germany, 1997.
[14] P. Manfrinetti, M. L. Fornasini, D. Mazzone, S. K. Dhar, and R. Kulkarni, J. Alloys Compd. **379**, 64 (2004).
[15] P. Manfrinetti, A. Palenzona, S. K. Dhar, C. Mitra, P. L. Paulose, D. Pal, and S. Ramakrishnan, J. Magn. Magn. Mater. **213**, 404 (2000).
[16] S. K. Dhar, C. Mitra, P. Manfrinetti, and R. Palenzona, and A. Palenzona, J. Phase Equilib. **23**, 79 (2002).
[17] S. K. Dhar, P. Manfrinetti, and A. Palenzona, Solid State Commun. **124**, 379 (2002).
[18] P. Svoboda, M. Divis, E. Gratz, R. Černý, and L. Dobiášova, Phys. Status Solidi A **123**, K149 (1991).
[19] M. Shiga, Physica B & C **149**, 293 (1988).
[20] L. Guènèe and K. Yvon, J. Alloys Compd. **356-357**, 114 (2003).
[21] J. O. Willis, R. H. Aiken, Z. Fisk, E. Zirngiebl, J. D. Thompson, H. R. Ott, and B. Batlogg, in *Theoretical and Experimental Aspects of Valence Fluctuations and Heavy Fermions*, edited by L. C. Gupta and S. K. Malik (Plenum, New York, 1987). p. 57.
[22] M. Divis, E. A. Goremychkin, P. Svoboda, V. Nekvasil, J. Bischof, and R. Osborn, Physica B **168**, 251 (1991).
[23] J. M. Barandiran, D. Gignoux, J. Rodriguez-Fernandez, and D. Schmitt, Physica B **154**, 293 (1989).
[24] L. D. Tung, K. H. J. Buschow, J. J. M. Franse, P. E. Brommer, H. G. M. Duijn, E. Brück, and N. P. Thuy, J. Alloys Compd. **269**, 17 (1998).
[25] T. Yamade, N. Kumitomi, Y. Nakai, D. E. Cox, and G. Shirane, J. Phys. Soc. Jpn. **28**, 626 (1970).
[26] R. W. Tustison and P. A. Beck, Solid State Commun. **20**, 841 (1976).